B. E. Argyle J. C. Slonczewski O. Voegeli

Bubble Lattice Motions Due to Modulated Bias Fields

Abstract: We observe that periodic variations of bias field can couple to a close-packed lattice of magnetic bubbles to produce a steady rotation of the bubble lattice (RBL). Pulsed fields excite various other many-body phases as well. The physical motions of such bubble arrays can be described by "lattice melting," "evaporation," and "rotating galaxies." The RBL phase is stable over wide ranges of pulse width and amplitude when the film is thick and the lattice is confined either by a circular ion-milled groove or by radially symmetric inhomogeneous fields from the excitation coil itself. Microsecond pulsed fields of $-0.05 \times 4\pi M_s$ applied to a lattice of five- μ m bubbles produce a net displacement of up to 1.5μ m/pulse at the rim of a lattice 23 bubbles across and 250μ m in diameter. Sinusoidal bias modulation in the range 1 to 30 MHz produces a spectrum of lattice rotational velocities vs frequency having both signs. At frequencies near the low end of the spectrum both the magnitude and the sign of the rotation are sensitive to drive amplitude. A tentative theory attributes lattice rotation to nonlinearities involving the bubble-deflection effect. The mechanism is strong enough to account for the observed magnitude of rotational frequency and can explain its resonant peaks and sign changes.

Introduction

Bubble domains are cylindrical regions of reversed magnetization in a thin film of material that is elsewhere polarized in a direction normal to the film [1]. Because of the ease with which magnetic bubbles can be manipulated and because of their microscopic size, circuits and experimental storage devices have been constructed and are being considered for possible application in memory devices.

The conventional means for positioning and translating bubbles employs local spatial variations of the bias field on a scale of the order of the bubble size [2]. These local fields are provided by overlaid current-carrying conductors or by magnetic Permalloy patterns that are magnetized by an externally applied rotating in-plane field. Bubbles as small as 800 Å in diameter have been observed with the electron microscope, but the potentially high storage density cannot be utilized because overlay patterns of similar dimensions have not been fabricated.

In the recently proposed bubble lattice file (BLF)[3], the positions of bubbles are maintained by interactive forces among bubbles rather than by overlaid elements, and bubble translation still relies on overlaid current conductors [4] of width comparable to bubble size. To maintain an ordered array, however, the information must be stored using two different types of bubbles rather than the presence or absence of bubbles as in the conventional bubble memory.

Two methods are being considered for storing information in the bubble. One utilizes two different stable arrangements of magnetization within the bubble wall and these can be discriminated by their dynamic characteristics [5]. Another proposal has been suggested whereby a conveyor layer maintains a periodic bubble array while data are represented in an adjacent storage layer by the presence or absence of bubbles coupled to the conveyor lattice. The two magnetic layers may be separated by an intervening layer of nonmagnetic garnet material [6].

This paper discusses a phenomenon we call bubble automotion whereby the bubble lattice is propelled by a time-modulated bias field, which varies smoothly over a long distance, rather than by locally applied field gradients, thereby eliminating the need for fine scale propagation structures.

The fact that unexpected bubble motions and modes of collective bubble translation can be excited in a bubble array by modulated bias fields has been noted previously in the literature [1-4, 7, 8]. When pulse modulated bias fields were used to "stain" defects in bubble films with the bubbles themselves [7], it was noted that local vibrational- and lattice-translational modes could be excited, depending upon the field-pulse shapes. Subsequently we found that a bubble lattice contained within the modulation coil could be caused to rotate coherently both by pulsed bias-fields (of either sign) and by rf sinusoidal fields [8]. Microwave fields generated locally with a pair of short-circuited slot lines have also been reported to produce rotations within a bubble array [9]. Related observations on isolated bubbles constrained to move parallel to the edge of a conductor have been made.

109

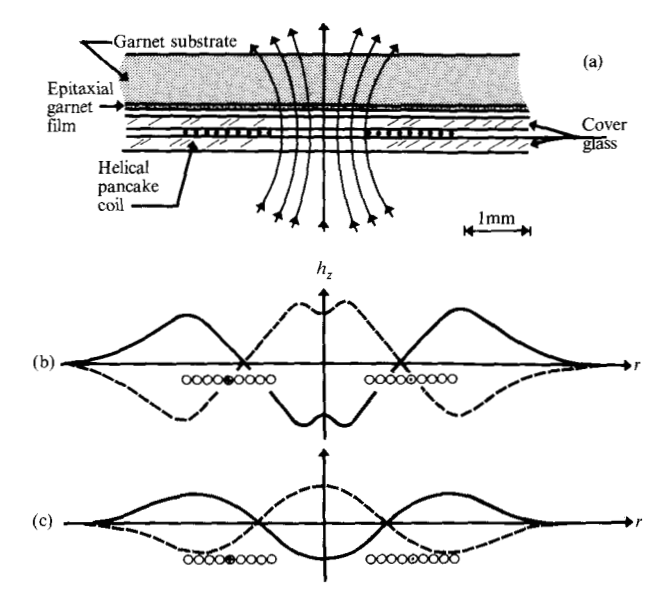


Figure 1 Experimental configuration and garnet specimen for exciting motions in bubble arrays. (a) Geometrical arrangement of film, substrate, and bias-field coil. (b) and (c) Effects of coil on lattice confinement. The lattice is confined either by a field-well shaped by the spiral modulation coil itself, as in (b) and (c), or by the circular etched groove depicted in Figure 2. The shape of $h_z(r)$ depends on film-to-coil separation, e.g., 0.15 mm in (b) and 0.38 to 0.50 mm in (c). Solid curves are for pulsed currents producing negative or bubble-expanding central fields, and dashed curves are for positive pulses. The combination of sign and film-to-coil separation determines the sign and strength of the radial gradient force.

Boxall [10] used pulsed gradients directed perpendicular to the allowed direction, while Hubbel [11] used pulsed-modulated ac currents in the constraining conductor itself to propagate the domains. Bias modulation applied to materials that can support hard bubbles is known to cause rotations [5, 12] of stripped-out hard bubbles (called propellers or dumbells) about an axis centered in their body. When hard bubbles are present as a minority in a lattice being translated by bias modulation they are carried along by the lattice, and when local-mode vibrations are excited within the bubble lattice, a visual display shows the hard bubble as being quiescent against the blurred background of normal bubble motion [13].

The present investigation characterizes the modes of motion induced in arrays of normal bubbles by both pulsed and rf-modulated bias fields. Under pulsed field excitations the motions observed can be classified according to specific ranges of the independent parameters, e.g., pulse duration and amplitude, where they occur. We name these mode-phases by analogy to chemical equilibrium phase diagrams, e.g., "liquid melt," "stationary lattice," "rotating lattice," "local mode vibrations," etc. Transition boundaries delineating these regions in the phase diagram depend upon steady state

parameters such as external fields, bubble film properties and, of course, the shape of the confining boundary potential. Our primary emphasis here is placed on the rotating bubble lattice (RBL) phase. The conventional single-layer material as well as the magnetostatically coupled layers of Lin, et al. [6] are investigated. The compositions are nominally $R_x Y_{3-x} Ga_y Fe_{5-y} O_{12}$, R being either Eu or Gd, $x \approx 0.7$, and $y \approx 1.1$.

In our initial approach to a theory, the rotation of the bubble array is ascribed to nonlinear dynamics connected with skewed translation of bubbles in a gradient field [5, 14]. In the case of pulsed-drive conditions, the steady term in the rotation is due to the inequivalence of the deflection angle for the two directions of bubble motion involved. In the case of sinusoidal excitation h_{z} = $h_{\rm p}(x, y) \sin \omega t$, where $h_{\rm p}$ is the peak value of field, the phenomenon is ascribed to a nonlinear coupling of the radial oscillations and the deflected translations. Both models neglect possible effects of in-plane, pulse-driven propagation [15] of unichiral bubbles and pulse-biasdriven spiral translations of bubbles containing clustered Bloch lines [16]. We observe separately the radial response and translational response, i.e., the RBL. The radial response is studied by Faraday photomagnetooptic detection of wall displacements while the translational response is simultaneously monitored, e.g., as a spectrum of rotational (RBL) velocities vs rf frequency.

The next section describes the various experimental situations and procedures. The third section gives results for the case of a lattice weakly confined by the time-averaged field-potential well from pulsed currents in a spiral pancake coil, and the section following describes detailed measurements on bubble lattices tightly confined by a circular groove etched into the garnet films. The fifth section demonstrates the rotating bubble lattice as well as dual bubble conversions in the composite layer of Lin, et al. [6], followed by some preliminary theoretical models for the RBL effect. The last section offers some additional interpretive discussion.

Experimental arrangement

Our experiments were carried out in a polarizing microscope. The arrangement includes bias-field and in-plane field coils. Static magnetic fields are read out digitally. Time dependent fields, produced by means of the flat spiral pancake coil shown in Fig. 1, have either pulsed, sinusoidal rf, or pulse-modulated rf form. Typically, the coil is constructed of #42 copper wire glued to cover glass 0.15 mm thick, and has one-ohm dc resistance and dimensions 1.5 mm I.D. and 3.5 mm O.D. Measured with a time domain reflectometer using 50-ohm termination, this coil has a fall time of about 2 ns and has an inductance of about 200 nH. The calibrated central field perpendicular to the plane of the film is nominally 4 × 10³ or

 2×10^3 A/m (50 or 25 Oe), respectively, per ampere flowing in the coil, depending on whether the specimen is mounted with film side against the cover glass as in Fig. 1(a), or turned over to provide separation by the substrate thickness (about 0.38 to 0.51 mm). The profiles of field component $h_z(r)$ for these two cases are sketched in Figs. 1(b) and 1(c).

Pulsed currents with about 20 ns rise time were supplied to the coil by a pulse generator, or rf currents were supplied by a variable frequency generator and an rf amplifier. Pulse modulated rf currents are obtained using a double balanced mixer gated by a second pulse generator. The rf amplitudes can be maintained constant by means of an automatic gain control amplifier and diode detector.

Radial bubble wall amplitude response was detected using Faraday photomagneto-optic detection. These signals were processed by an amplitude response analyzer described previously [17]. The analyzer uses a sine-modulated carrier to measure the slope $dx/dh_{\rm p}$ of the wall displacement induced by the carrier frequency $\nu_{\rm rf}$ at amplitude $h_{\rm p}$. When the analyzer is applied to bubble radial oscillations R(t), the slope response $dR/dh_{\rm p}$ (proportional to peak response $R_{\rm p}$ within a linear region) is plotted automatically vs sinusoidal frequency $\nu_{\rm rf}$ in a swept frequency mode with $h_{\rm p}$ fixed.

Angular velocity of the rotating bubble lattice is determined and plotted vs rf frequency. Pulse modulation of the rf is used to slow the RBL rotation so that the time of one complete revolution can be visually observed. A dc voltage proportional to frequency is supplied by the variable frequency generator to the x axis of an xy recorder. The y axis monitors time sensed by a ramp generator voltage to allow the rotation period to be recorded by means of a "pen-down" signal initiated at a control box by the observer, the start of the ramp voltage having been previously initiated at the start of the rotation. The rotation period as a function of rf frequency has a spectrum that depends upon external parameters, e.g., bias field, in-plane dc field, size of lattice confinement, etc., as well as on amplitude of the rf drive. Pulsed field rotations are measured similarly, and the rotation per pulse found by dividing net rotation $\Delta\theta$ by the number of applied pulses monitored by a digital counter operated in the totalizing mode.

◆ Lattice confinement

Two successful means of confining the bubble lattice include (1) the weak field-well of the spiral coil itself [Figs. 1(b), (c)], and (2) the strong, sharp barrier of a thin circular groove [18] etched or ion milled into the surface of the epitaxial film as shown in Fig. 2. In regard to (1) it could be useful to have two coils, one for confinement and one for modulated bias. We have used only a

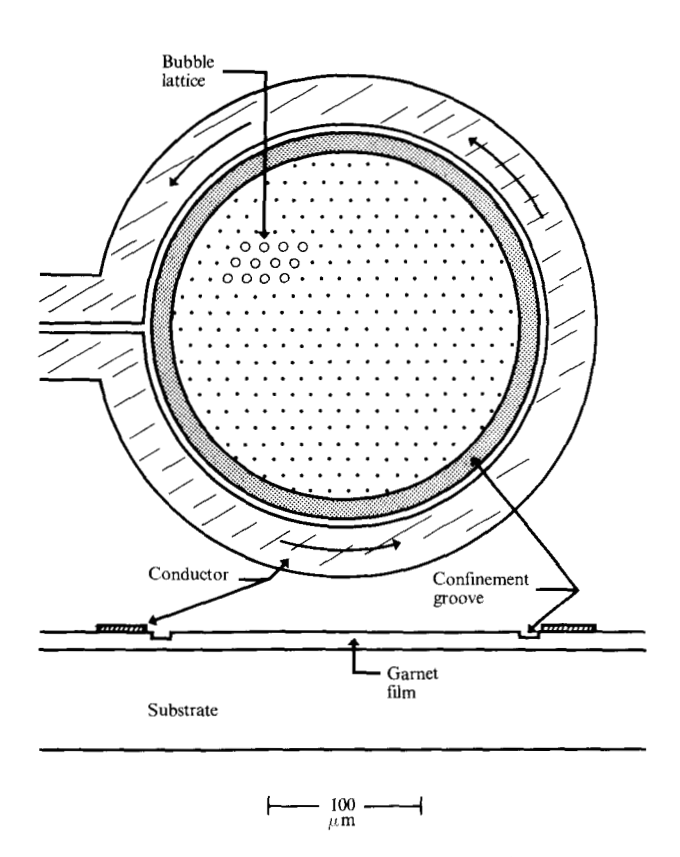


Figure 2 Example of lattice confinement by circular etched groove. A dc current applied to the circular conductor reduces "friction" forces of magnetostatic interaction with domains lying outside the groove.

single coil because the effect on the bubbles of the time average of unipolar pulsed field trains is suitable for confinement. In experiments involving etched groove confinement we also utilize the modulation fields supplied by the spiral coil. The circular confinement groove is, of course, smaller in diameter than the pancake coil.

Field wells generated by the spiral coil illustrated in Figs. 1(b) and 1(c) are for two sample-to-coil spacings (exaggerated). The (solid, dashed) lines result from currents producing (negative, positive) central fields. In the case of Fig. 1(b) bubbles would be (attracted, repelled) to the center for currents producing (positive, negative) central fields. However, the reverse situation occurs when the increased film-to-coil spacing in Fig. 1(c) is used. In addition to the opposite signs for currents to produce an attractive central force potential, other important differences in Figs. 1(b) and 1(c) include (1) the different ranges of confinement as delineated by the rim of the field-well, where $\partial h_r/\partial r \rightarrow 0$, and (2) the difference in strength of the confinement force, which for bubbles is proportional to $\partial h_z/\partial r$. A practical advantage of the negative central field well in Fig. 1(c) is that in the outlying region (r > r') beyond the

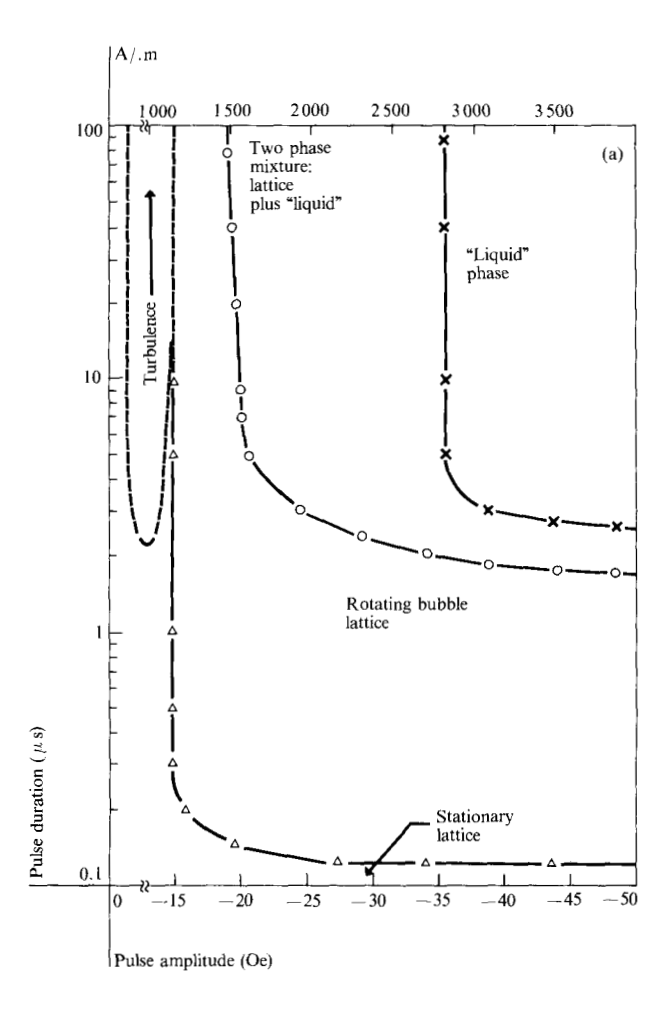




Figure 3 Chart analogous to chemical equilibrium phase diagram. (a) "Phase diagram" for modes of bubble motions observed and plotted in space of pulse amplitude vs duration for $Eu_{0.77}Y_{2.23}Ga_1Fe_40_{12}$ bubble film 12.6 μ m thick. Confinement and isolation is achieved by means of weak field-well (solid line) in Figure 1(c). (b) Streak photograph of rotating bubble lattice [RBL phase in (a)].

crossover circle defined by $h_z(r')=0$, i.e., the region where $h_z>0$, bubbles can be erased (i.e., collapsed). Thus, lattice isolation is accomplished coincidentally with lattice confinement.

Observed responses of bubbles to pulsed currents indicate that a profile like that of Fig. 2(a) occurs when the coil plane is separated from the film by the thickness of a 0.15 mm coverglass, as shown in Fig. 1(a). The field well in Fig. 1(c) results when the separation is increased by an additional 0.38 to 0.50 mm, i.e., the substrate thickness with the sample turned over.

To investigate the RBL phase in detail requires suppressing other phases and preventing the bubble escape that can occur in the weak field-well confinement. Because of the resulting discontinuity in the domain wall energy, a strong, steep boundary potential is provided by the etched groove with steep sides [18], illustrated in Fig. 2. To avoid bubble interactions with defects at the imperfect groove, it is also desirable to repel the bubbles from the edge. This can be done by adjusting the width of the groove to accommodate the width of a stripe domain, thus allowing a trapped stripe to repel the bubbles from the groove. Alternatively, a dc current may be applied to the conductor loop of Fig. 2 to collapse domains inside the groove and shrink bubbles near the rim of the rotating lattice, thus reducing magnetic-dipole interactions with domains outside the lattice.

Pulsed-field modes with weak field-well confinement

Using the weak field wells of Fig. 1 we observed various modes of bubble motion, which were dependent on pulse width and amplitude and, to a lesser extent, on the strength of the uniform bias field and on the repetition rate. Figure 3(a) characterizes these modes in terms of a mode-phase diagram (analogous to an equilibrium phase diagram) with measured boundaries separating the phases, e.g., "liquid," "stationary lattice," "rotating lattice," and "turbulence." The rotating lattice is streakphotographed in Fig. 3(b), and names ascribed to the other motions are appropriately descriptive. For example, the "liquid" phase occurs when local mode vibrational translations of the bubbles attain amplitudes sufficient to destroy the hexagonal lattice. In the "turbulence" phase, large velocity translations of bubbles and collections of bubbles occur in seemingly random directions, thereby breaking up the lattice characteristically. In an unmarked region near the middle of the RBL in Fig. 3, phase changes in density and lattice spacing occurred because some bubbles escaped or collapsed in the region under the coil.

A result found by investigating a variety of garnet films is that mode stability and phase boundary reproducibility are greater in thicker films and films with smaller tilt of the [111] crystal axis from the film normal. The film used for Fig. 3 is relatively thick (12.6 μ m compared to the value of the material length parameter, $l=0.66~\mu$ m), has a tilt of 0.3°, and has composition Eu_{0.77}Y_{2.23}Ga, Fe₄0_{0.2} and $4\pi M_s = 1.75 \times 10^{-2}$ T (175 G).

The procedure for taking data consists of placing the sample, usually with film side away from the coil to provide the field well in Fig. 1(c); adjusting the bias in the range of bubble stability; and "chopping" stripe domains using pulsed fields to produce a bubble lattice [19]. The types of collective bubble motion induced by negative pulse trains are then observed, and the transitions between "phases" are noted while adjusting pulse duration and amplitude and are plotted in the space of independent parameters as in Fig. 3(a).

Pulse duration, amplitude, and sign are the most significant parameters, the latter affecting the sign of the radial gradient force (proportional to $\partial h_z/\partial r$) as indicated in Fig. 1. The bias field, although expected to have some effect on the radial spring constant $\partial R/\partial h_z$ of the bubble, has rather slight effect on the phase boundary positions. Pulse repetition rate affects primarily the velocity of motion and not very much the positions of the phase boundaries. However, high repetition rate in combination with large pulse durations can shift the effective dc bias field. The phase diagram in Fig. 3(a) was obtained by using relatively low repetition rates of about 500 pps, and bias adjustments were not required.

The "turbulence" region in the phase diagram has its own interesting characteristics. This region is broader in width for thinner samples, thereby encroaching on the RBL phase in Fig 3(a). Also, within this turbulence region other modes have been observed. These modes include contra-rotating lattice ("eddys"), and sometimes a second coherent RBL phase with sense of rotation opposite to that observed in the rotating bubble lattice area in Fig. 3(a). The types of mode observed within the turbulence region also depend very sensitively on pulse amplitude.

The RBL effect has been observed in most of many films studied which, like the sample in Figs. 2 and 3, have low damping, α being approximately 0.1. Extra thin samples $(h/l \le 2)$ did not exhibit this RBL phase. Gradient pulse propagation measurements on bubbles exhibiting the RBL effect in Fig. 3 show that these bubbles have small winding numbers [11, 26] $(S = 0, \pm 1)$, high mobility $(\mu \gtrsim 800 \text{ cm/sec-0e})$, and high saturation velocity ($\gtrsim 800 \text{ cm/s}$) occurring when the drive force $\nabla H_z = d\partial H_z/dr$ equals 23 to 30 A/m (3 to 4 Oe). It has not yet been determined which ranges of these quantities are necessary and/or sufficient for the film to exhibit the RBL phase. We are certain, however, that in lattices of very hard bubbles the RBL response is absent. Although it is known that a striped-out hard bubble can respond to pulsed bias by rotating around an axis through its body [5], we have observed that lateral translation is generally absent.

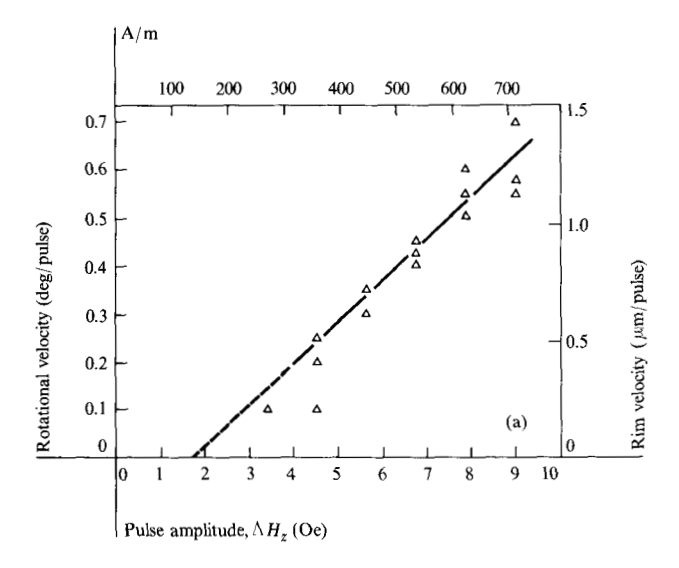
To examine effects of changing the shape of the field well, the field well in Fig. 1(b) is obtained by turning

the sample over so that the film plane is placed adjacent to the coil. With positive field pulses now applied, new modes that might be called "rotating galaxies" and "evaporation" are observed. The field well, now having a smaller rim radius, contains fewer bubbles, and, having weaker central forces because $\partial h_z/\partial r$ is smaller, allows larger equilibrium bubble-to-bubble spacings. Consequently, long-range order within the bubble array is relaxed and is disturbed by coercive forces. Because of the visual appearance, the result can be termed a "galaxy." Nonetheless, the galaxy can be rotated. The concept of phase boundary is no longer applicable in this configuration because increased pulse heights greatly alter the number of bubbles by collapse. Borrowing the term "evaporation" seems appropriate, since bubble collapse occurs at the extremities of the galaxy near the range of pulse heights sufficient to rotate the galaxy and is accompanied by little apparent "melting".

Rotating lattice confined by circular etched groove

To make a detailed study of the RBL phase we have suppressed other phases and prevented bubble escape using the circular etched groove. The groove configuration provides confinement with a sharp potential discontinuity. In this study we (1) measured the angular rotation velocity in response to pulsed fields, (2) obtained its velocity spectrum in response to rf sinusoidal excitation, (3) investigated the effect on the results in (2) of applying an in-plane dc field, and (4) determined the bubble radial breathing mode response averaged over the lattice both when the lattice rotates freely and when it is "clamped" between a pair of long parallel grooves.

The sample with the circular confinement groove in Fig. 2 has composition $Eu_{0.7}Y_{2.3}Ga_{1.1}Fe_{3.9}0_{12}$, a thickness of 3.6 μ m, a $4\pi M_s$ value of 1.75×10^{-2} T (177 G), and a parameter l of 0.56 μ m. The response to pulsed bias given in Fig. 4(a) is a plot of angular rotation rate versus pulse amplitude. Data were taken up to the point at which lattice distortions, e.g., shearing, take place. The bubble size and lattice spacing are nominally 7 μ m and 11 μ m, respectively. The bias field (about 3.26×10^3 A/m, or 41 Oe), and pulse width (about 0.46 μ s) where chosen optimally, i.e., for maximum rotation rate and minimum hesitation and lattice distortion. Interaction with outlying domains was eliminated by using 100 mA dc current in the concentric conductor strip line shown in Fig. 2 so as to collapse domains lying in the groove and shrink the circular layer of peripheral bubbles that accommodates the angular boundary of the hexagonal lattice to the circular shape of the confinement groove. The maximum bubble velocity, 1.5 μ m per pulse [right-hand ordinates in Fig. 4(a)], observed at a rim having a radius of 125 μ m, appeared limited by lattice shearing. Although this distortion might have been avoided by a more



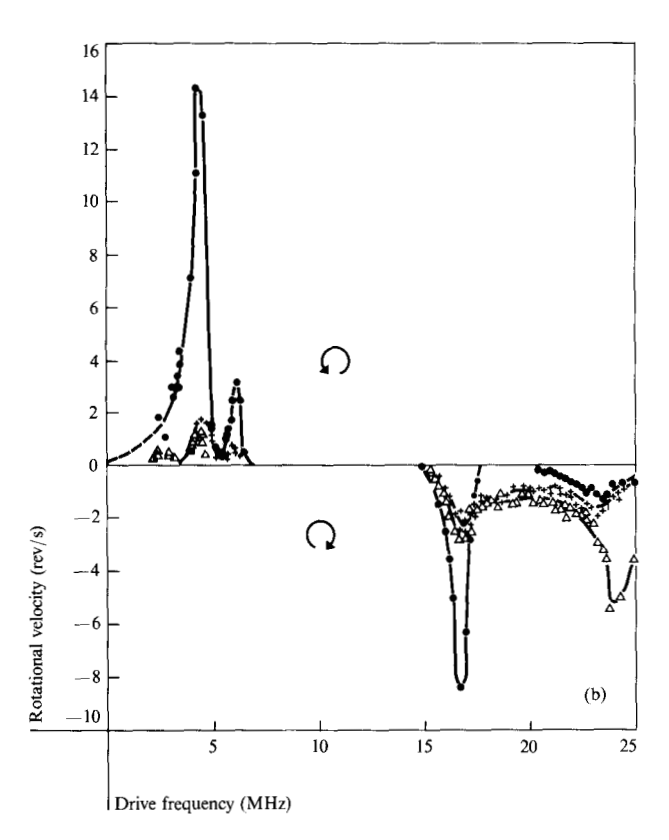


Figure 4 Pulse and sinusoidally driven response of lattice confined by circular groove 250 μ m in diameter, shown in Figure 2. (a) Angular velocity vs pulse amplitude obtained using pulse width of 0.46 μ s. Right-hand scale gives velocity per pulse for bubbles at the rim of the lattice. Circular conductor with 100 mA dc current reduce magnetodynamic "friction" (see text). Bias field applied is 1.43×10^3 A/m. (b) Sinusoidally driven lattice rotational velocity vs drive frequency with fixed rf peak drive $h_p = 1.03 \times 10^3$ A/m and in-plane field of zero (·), 239 (Δ), and 478 (+) A/m, respectively. Applied bias is 5.71×10^3 A/m. Bubble film of (Y, Eu) $_3$ (Fe, Ga) $_50_{12}$ has $4\pi M_s = 1.77 \times 10^{-2}T$, $\ell = 0.56$ μ m, thickness, 3.6 μ m, and field where isolated bubble collapse, 6.17×10^3 A/m.

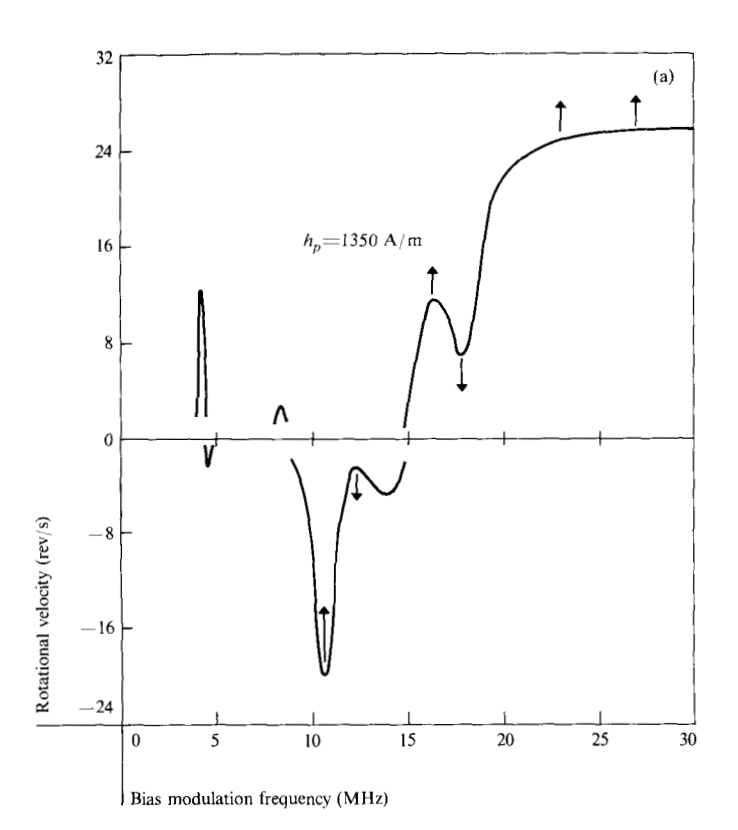
suitable choice of field-well, it is possible that the threshold for nonlinear velocity response had been exceeded.

Bursts of pulses 715 A/m \times 0.46 μ s with fixed separation produced rotational rates that depended linearly on the pulse rate up to the point that separation approached the pulse duration. At a pulse separation smaller than about 1.0 to 1.5 μ s the motion became erratic and stopped. The corresponding threshold velocity for the outlying bubbles is given by the average 1.5 μ m/pulse \div 1.5 μ s/pulse, or about 100 cm/s, deduced by assuming that outlying bubbles maintain the average velocity per pulse in the repeated single pulse data of Fig. 4(a). The corresponding rotational velocity at this threshold is about 1300 revolutions per second.

The RBL spectrum obtained for this sample in response to sinusoidal drive is given in Fig. 4(b) and was produced with the pancake coil in Fig. 1 in a fixed dc bias field of 5.73×10^3 A/m. The amplitude of rf field is 1.08×10^3 A/m peak, measured at the center of the pancake coil. The 250 µm circle diameter is small compared with the pancake coil I.D. of about 1.5 mm. The ordinates in Fig. 4(b) are adjusted for a 10 percent duty cycle of pulse-modulated rf used to slow the RBL rate to a measurable value. In the absence of in-plane dc field, four sharp peaks in lattice rotation rate occur: two counterclockwise (ccw) rotations at 4.3 MHz and 6.2 MHz and two clockwise (cw) rotations at 16.8 MHz and 23.5 MHz. The maximum rotation rate, 15 rev/s at 4.3 MHz, corresponds to 1.2 cm/s bubble velocity at the rim. This magnitude is small in comparison with isolated bubble velocities up to 1600 cm/s observed by pulsed gradient propagation in this film and is also small compared with 1.5 μ m/pulse observed in Fig. 4(b).

It is known that in-plane fields play a significant role in the behavior of domain wall structure and dynamic response [19-22]. Applying small, constant in-plane fields ($H_{\rm ip} = 3$ and 477 A/m in Fig. 4(b)) suppresses the rotation peaks driven at 4.3, 6.2, and 16.8 MHz and enhances and broadens the peak at 23.5 MHz. Beyond an $H_{\rm ip}$ value of about 800 A/m the rotation stops or becomes incoherent.

A 3/4 mm diameter groove was milled into another garnet film 11.5 μ m thick, having composition $Gd_{0.6}Yb_{0.7}Y_{1.7}Ga_1Fe_4O_{12}$, and values of $l=0.62~\mu$ m, $4\pi M_s=1.3\times 10^2$ T, and Q=4. The RBL spectrum given in Fig. 5(a) was obtained using $h_p=1.59\times 10^3$ A/m and $H_{1p}=0$. The rim bubbles attained a velocity of at least 25 rev/s. Application of 560 A/m of in-plane field increased this to about 30 cm/s. Vertical arrows indicate other shifts induced in the spectrum by this in-plane field. For example, we observed enhancement and sharpening of the peaks at frequencies near 16 MHz and beyond 20 MHz. Below about 10 MHz the RBL structure was unstable,



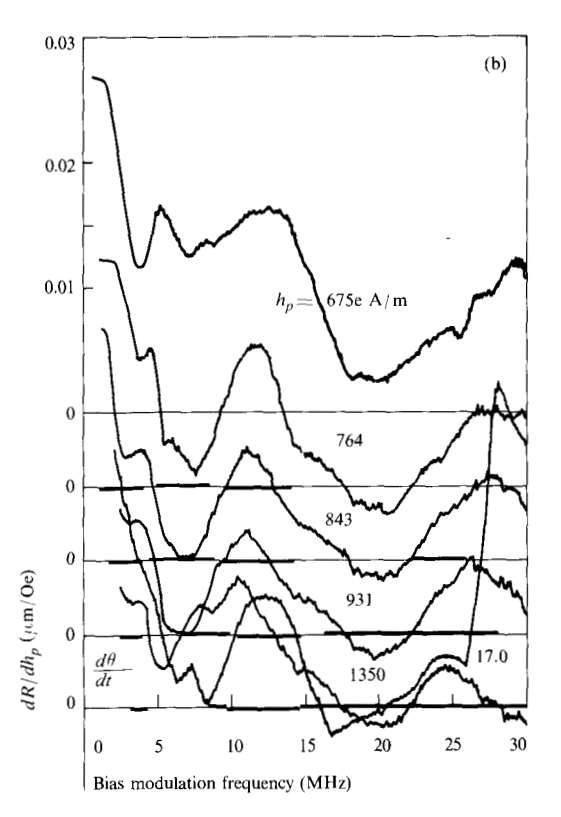


Figure 5 Sinusoidally driven response of lattice contained within 0.75 mm diameter groove vs frequency. (a) Angular rotation rate for $h_{\rm p}=1.35\times10^3$ peak rf. (b) radial bubble wall displacement envelope response derivative $dR/dh_{\rm p}$ for several $h_{\rm p}$ (measured using 15 percent amplitude modulated rf); frequencies where (positive, negative) rotations occur are denoted by solid bars (bars, below) the axis. Comparison of $dR/dh_{\rm p}$ data when bubble lattice is not free to rotate is given by heavy line for case $h_{\rm p}=1.35\times10^3$ A/m. Bubble film has composition ${\rm Gd_{0.7}Yb_{0.7}Y_{0.7}Y_{0.7}Y_{0.7}A_{\rm p}}$, $4\pi M_{\rm s}=1.3\times10^{-2}{\rm T}$, $\ell=0.62~\mu{\rm m}$, thickness is 11.5 $\mu{\rm m}$, and tilt is 0.6 degrees from [111] normal. Bias field applied is 5.49×10^3 A/m. The lattice contains bubbles about 9 $\mu{\rm m}$ in diameter, with 30 $\mu{\rm m}$ spacing.

i.e., the frequency position and sign of the rotation peaks shifted nonmonotonically and sometimes discontinuously with both H_{in} and drive h_{in} .

Wall radial response In absence of in-plane fields, if all bubbles in an infinite lattice consisted of one kind of wall structure, their dynamic radial wall response to a uniform modulated bias would have a common phase and exhibit cooperatively a single resonance [23, 24] (or relaxation) whose position in frequency would depend upon the radial restoring force, therefore on $\partial R/\partial H_z$, and on the mass of the wall (or the damping). In all materials studied the damping is small and nonlinear wall response can be expected [17, 19-22]. The Döring mass frequency of about 1 to 40 MHz is well below the expected relaxation frequency because of damping. For multiple types of bubble walls [5, 12, 14, 25, 26], e.g., bubbles with and without vertical Bloch lines, one would expect spectra with multiple peaks reflecting these various wall structures. Other peaks allowable because of finite boundaries may occur as well.

Measurements of mean dynamic radial amplitude response dR/dh_p of bubbles in a free rotating lattice are

presented in Fig. 5(b), which also shows the response when the lattice is "clamped" between a pair of parallel grooves. The physical meaning of $dr/dh_{\rm p}$ measurements can be understood as in previous work on straight wall response [17]. In response to a modulated rf field

$$h_{\nu}(t) = h_{\nu}[l + m \sin \omega_{0} t] \sin 2\pi \nu_{\rm rf} t, \tag{1}$$

the radial wall response may be written

$$R(t) = R \sin (2\pi \nu_{\rm rf} t + \phi)$$

where, for small modulation $(m \ll 1)$ the envelope is given by

$$R = R_{\rm p} + \frac{\partial R}{\partial h_{\rm p}} m h_{\rm p} \sin 2\pi \nu_0 t$$

$$+ \frac{1}{2} \frac{\partial^2 R}{\partial h_{\rm p}^2} (m h_{\rm p} \sin 2\pi \nu_0 t)^2 + \cdots. \tag{2}$$

The displacement amplitude $R_{\rm p}$ corresponds to the peak field $h_{\rm p}$, $dr/dh_{\rm p}$ is the slope of the radial wall displacement vs peak drive $h_{\rm p}$ evaluated at the frequency $\nu_{\rm rf}$ and the peak $h_{\rm p}$, and ν_0 is the low frequency modulation, e.g., 1 kHz. The measuring system processes the PMT sig-

nals (proportional to Faraday contrast and wall displacement) and synchronously detects the second term in (1), producing a dc signal proportional to $dR/dh_{\rm p}$. Therefore, while a frequency spectrum observed to be independent of $h_{\rm p}$ would indicate linear oscillator behavior, this system monitors nonlinear behavior as well.

The swept frequency data in Fig. 5(b) were obtained using 15 percent modulation for m and several fixed values of h_p . The RBL effects observed simultaneously with $d\mathbf{R}/dh_{\rm p}$ are indicated by solid bars above and below the axes to show at which frequencies the positive and negative rotations occur. The multiple-peaked structure as a function of frequency suggests the presence of more than one type of bubble wall. Nonlinearities in radial response, i.e., deviations from a linear relationship of R vs $h_{\rm p}$, are indicated by variations in sign and magnitude of dR/dh_p with changes in drive peak h_p . According to Fig. 5(b) the average bubble in the lattice exhibits (1) decreased slope dR/dh_p with increased drive h_p , and (2) negative slopes $(dR/dH_{\rm p} < 0)$ occurring at high frequencies, i.e., about 20 MHz when h_p is more than 715 A/m and higher than 30 MHz when h_p is greater than about 950 A/m.

Previous measurements of high-frequency-driven parallel wall displacements have shown that even for small displacements the peak envelope response x_p varies nonlinearly with drive $h_{\rm p}$, and depends on the in-plane field H_{in} . The range of linear dependency on h_{in} increases as frequency increases. At higher drive fields negative dx/dh_p occurs, showing that x vs h_p is a peaked response. Interpretation in terms of a threshold velocity V_0 determined by using $V_0 = 2\pi v_{\rm rf}$ was suggested by the observed decrease in threshold x_0 of departure from linearity with increase in frequency ν_{rf} . Velocity thresholds, observed in garnet films with low damping, are similar to predictions [5] for nucleation and annihilation of horizontal Bloch lines, i.e., an energy dissipation mechanism accompanied by loss in momentum. Applying an in-plane field raises this threshold velocity and decreases the wall mass [19-21].

Wall motion response in bubbles, Fig. 5(b), is even more complex than in parallel stripe domains, presumably because of multiple wall states in bubbles. Individual bubble wall states can be characterized by experiments measuring propagation deflections [5, 14] in a pulsed gradient field. We have propagated bubbles taken individually from the rotating lattice and find the types are limited usually to winding numbers S=+1, as for unichiral bubbles, and S=0, as when two Bloch lines of like sense are present. An in-plane field, e.g., a field due to tilt of the crystal (111) axis from the film normal, or just an applied in-plane field, may further subdivide these states and perhaps account for the observed multiplicity of response to modulated bias.

The preliminary results in Fig. 5(b) suggest the presence of perhaps five or six peaks in the $dR/dh_{\rm p}$ data and six peaks of lattice rotation appear in the RBL spectra of Fig. 5(a). The sample tilt is 0.6° and we may estimate an internal in-plane field of about 3.18×10^{3} A/m for this sample.

Where the difference between radial amplitude response for a clamped and for a freely rotating lattice is large, i.e., near 25 to 30 MHz in Fig. 5(b), the RBL rotation velocity is also large. Moreover, the radial amplitude response in the free lattice is strongly nonlinear, e.g., dR/dh_p is even negative at drives beyond $h_p = 715 \text{ A/m}$ and frequencies beyond the point where ν_{rf} is about 28 MHz. These results suggest that, for these higher frequencies at least, nonlinear coupling between the radial and translation degrees of freedom of bubbles is responsible for a large share of the force driving the RBL motion.

Effects of pulsed bias on bubbles in magnetostatically coupled films

The bubble lattice file thus far encodes information with different wall states for bubbles, i.e., different numbers of Bloch lines [3]. An alternative scheme involves bistable, dual-size bubbles that can coexist in a common bias field but possess different sizes. Bistable bubbles have indeed been observed in films with gradients in composition [27, 28], in bilayer films [28, 29], in trilayer films with a nonmagnetic middle layer [6], and in multiple-layered films with compensation wall boundaries [30]. Since the energy barrier separating the two states of a dual-sized bubble includes wall surface energy rather than Blochline or Bloch-point energy, information stored in this way may be more stable than in the case of wall-state storage. The requirement of a uniform lattice periodicity for practical devices is optimized in one of these layered structures. In most cases the size and/or height difference in the two types of bubble causes difference in bubble-to-bubble spacings. The exception occurs in one of the trilayered films of Lin, et al. [6] shown in Fig. 6(a) and 6(b), the so called "intermediate coupling case." The thick bottom layer in one of their "composite c" samples [6] supports a lattice of large bubbles, and the binary information storage occurs according to the presence or absence of a small bubble in the top layer magnetostatically coupled to the bottom layer bubbles. The lattice spacing is largely unaffected by the absence or presence of bubbles in the top layer. Uniform lattice spacing is demonstrated in the Faraday-effect photograph, Fig. 6(a), exhibiting a random distribution of such bistable states within an equilibrium lattice configuration. The analyzer and polarizer have been set at an offset angle suitable to produce black and white bubbles against a gray background.

To write information into such a lattice, after first nucleating the lattice of large bubbles in the bottom layer, requires controllable nucleation of small bubbles in the top layer at the positions where "ones" instead of "zeros" are to be stored. We have discovered that this kind of switching of an entire lattice is produced by means of pulsed bias fields of negative sign with respect to the uniform dc bias field having suitable width and amplitude. To switch a single bubble in the presence of others, however, has not been attempted. Random switching, as in Fig. 6(a), can be produced at the switching threshold [Fig. 6(c)]. The locus of points (pulse amplitude versus width) specifying the threshold where the transition (uncoupled bubble → coupled bubble) occurs is presented in Fig. 6(c), in the curve marked " $1 \rightarrow 3$." Similarly, positive pulsed fields cause conversions $3 \rightarrow 1$ at amplitudes and widths beyond a somewhat different threshold curve. The uniform bias was held fixed at 6.127×10^3 A/m, which is convenient for maintaining a stable, equilibrium bubble lattice in the bottom layer.

Bubble lattice automotion carrying these dual bubble states can also take place in this composite film; it occurs within the rather broad region of negative pulsed fields indicated in Fig. 6(c).

It is remarkable that automotion and bistable-bubble state transitions can occur at different pulsed bias conditions, because this implies that in this memory scheme the three functions of read-in, read-out, and lattice translations can be performed independently of each other. In particular, pulses producing lattice automotion will not disturb the stored information if chosen with suitable amplitude and width as indicated in Fig. 6(c).

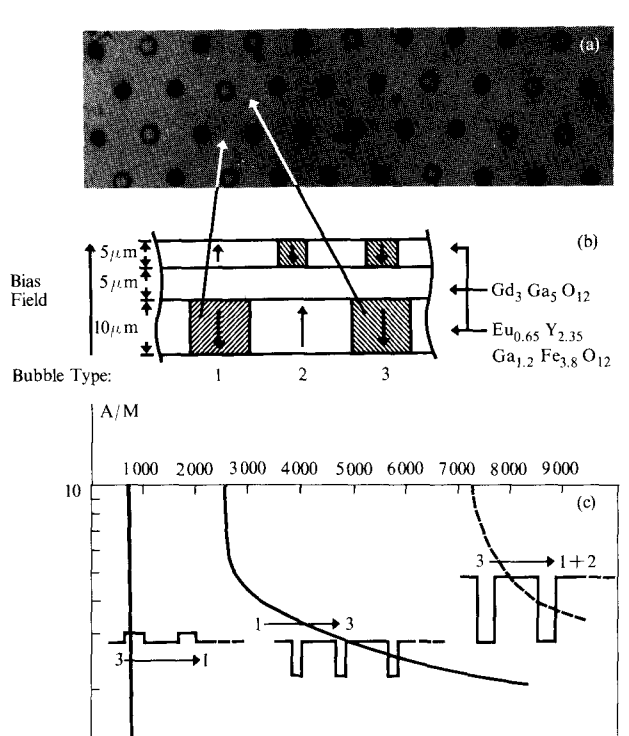
Mechanism of lattice rotation

The problem of explaining the rotation of a bubble lattice may be posed thus: Inhomogeneity of the field component (normal to the film) produced by the drive coil implies the presence of a gradient ∇H_z necessary to displace bubbles. ∇H_z is directed radially from the axis of rotational symmetry common to the coil, the center of the bubble array, and its confining structure if such is present.

There are two parts to the problem. First, if ∇H_z has a radial direction, how can it produce a velocity in the orthogonal direction corresponding to rotation of the lattice? This question is naturally answered in terms of the well-known gyrotropic force F, which causes the bubble-deflection effect [5, 31]. It is given by

$$\mathbf{F} = 4\pi M_{\circ} \gamma^{-1} S \hat{z} \times \mathbf{V}, \tag{3}$$

where \hat{z} is a unit vector normal to the film plane and V is the instantaneous velocity of the domain. Here S is the state, or winding, number of the domain wall. It is given by the number of complete rotations executed by the in-plane component of the magnetic vector within the



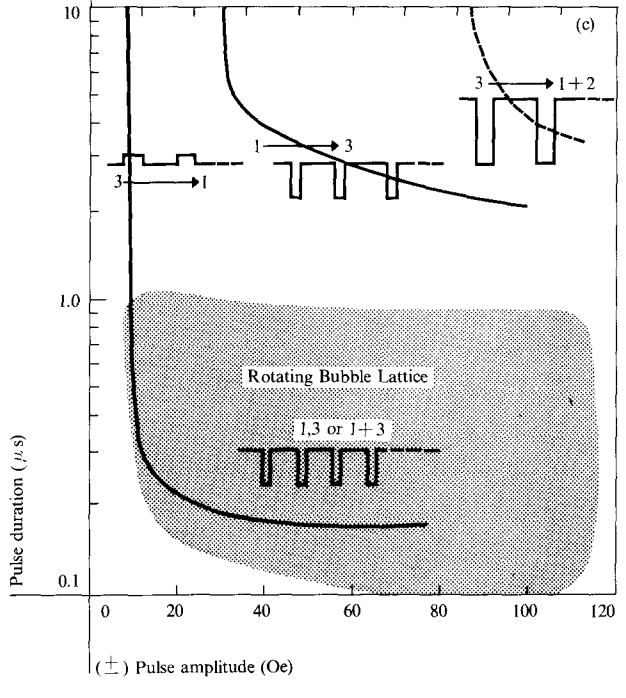
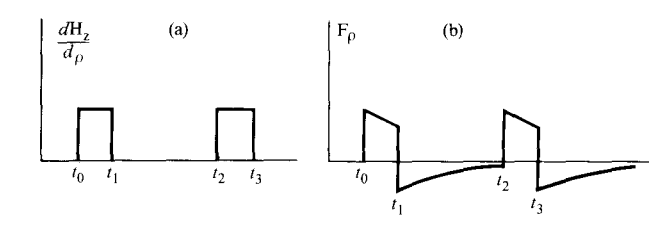


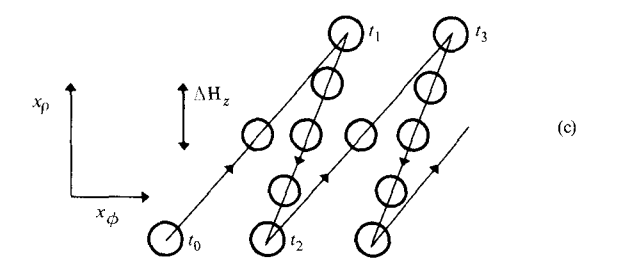
Figure 6 Lattice automation and state switching in composite magnetostatically coupled film of Lin, Grundy, and Giess [6]. (a) Faraday contrast photograph of bistable bubbles, (b) designated states of coupled and uncoupled bubbles, (c) thresholds for conversions among bubble states in (b) and phase region (gray area) for bubble lattice automotion. Conversion by (collapse, nucleation) of top bubble at site of permanent bottom bubble are induced at solid lines $(3 \rightarrow 1, 1 \rightarrow 3)$ or beyond. Dashed-line threshold $(3 \rightarrow 1 + 2)$ indicates where top bubble is decoupled from bottom bubble.

domain wall in one circuit of the domain. It is also related to the net vertical-Bloch-line number n by

$$S = 1 + (n/2). (4)$$

In case Bloch lines of more than one sense are present, $n (= n_+ - n_-)$ is the net of n_+ positive and n_- negative lines present in the domain wall. The winding number S = 1, and corresponding deflecting force, occur in the absence





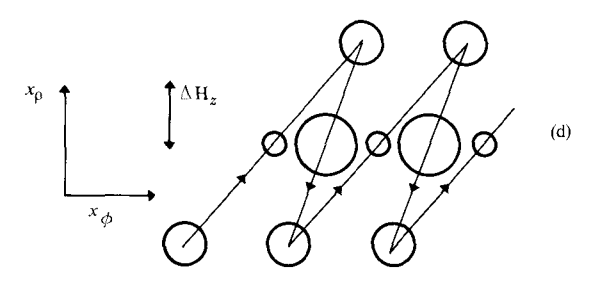


Figure 7 Asymmetric drive condition: (a) Applied asymmetric radial field gradient vs time t for pulsed drive. (b) Net radial force on bubble vs t. (c) Lattice rotation mechanism for asymmetric drive shown in (a). Bubble positions at equal time intervals are shown. The forward and reverse deflection angles differ because the corresponding net forces differ, providing a net displacement X_{ϕ} per cycle. (d) Lattice-rotation mechanism for symmetric sinusoidal drive. The bubble responds to simultaneous uniform gradient and sinusoidal z fields. The effect of the gyrotropic force is greater when the bubble diameter is smaller, providing a net X_{ϕ} -displacement per cycle. Both radial and translational amplitudes are greatly exaggerated.

of Bloch lines because of the natural twist of the wall moment, which is tangent to the wall surface in a simple Bloch wall [16, 32].

The pulsed and alternating field strengths used in the present experiments are known from previous experiments to be sufficient to cause changes in S [5]. Since the bubble energy increases with $n_+ + n_-$, it is reasonable that the average value of n is zero. Therefore, the average S is 1 and we assume this value throughout.

The second part of the problem is this: Granted that transient or alternating lattice rotations arise from the deflection effect, how does a steady rotation arise? This can come about only from some nonlinearity in the system and must be discussed separately for the two cases of asymmetric and symmetric drive considered below.

• Asymmetric drive

Here we consider that the drive coil carries a train of identical current pulses of one sign, producing a similar radial gradient $dH_z/d\rho$ as shown in Fig. 7(a). Since a steady component of radial motion is not possible, the net force F_ρ acting radially with respect to the coil axis, including the effect of interbubble interactions and restraining barriers, must have both signs, as indicated in Fig. 7(b). Indeed, under simple assumptions the time average of F_ρ would vanish.

If the pulse width is not equal to one-half of the cycle time, then a steady component of velocity V_{ϕ} orthogonal to F_{ρ} arises from the velocity dependence of the bubble-deflection angles δ arising from coercivity and other nonlinear effects. For velocities below the critical instability value $V_{p} = 24 \ A/hK^{1/2}$, δ is given by the expression (for S=1) [5]:

$$\cot \delta = (\alpha R/2\Delta) + (2\gamma H_{e}R/\pi V). \tag{5}$$

This expression varies from $\delta = 0$ at $V \to 0$ to a maximum value

$$\delta_{\text{max}} = \arctan 2\Delta/\alpha R \tag{6}$$

at large V. Here R is the bubble radius, $\Delta = \sqrt{A/K}$ is the wall-thickness parameter and H_c is the coercivity. Although the V dependence of δ has not been tested experimentally for such a small value of S, the corresponding expression for large S is well established in hard bubbles (large X) for velocities below that required for Blochline annihilation [33]. However Eq. (5) cannot be relied on at drives exceeding that required to reach V_p . In any case, it is clear that δ does depend significantly on drive and that Eq. (6) represents its maximum value. This fact combines with the asymmetry in F_ρ to provide a net displacement per pulse orthogonal to F_ρ because of the difference in δ values for the two signs of F_ρ , as indicated schematically in Fig. 7(c).

The sign of the gyrotropic force is such that in a deflection experiment the sign of $S H_{\text{bias}} \cdot F \times V$ is always positive. If the pulse duration in our lattice rotation experiment is less than the time between pulses, then the average of $|F_o|$ is greater during the pulse than otherwise. Equation (5) shows that $|\delta|$ is then also greater during the pulse, if $V < V_{\rho}$ holds. Under this restriction, the condition $F_0 > 0$ would imply a right-hand screw relation of lattice rotation to H_{bias}. Actually left-hand lattice rotation is observed in the weak-field-well experiment with the negative pulsed field configuration of Fig. 1(c), at the threshold for uniform rotation. This result is consistent with our model, for $dh_z/d\rho > 0$ implies $F_o < 0$, although it must be remembered that the superimposed bubbleexpanding tendency of $h_z < 0$ favors the opposite direction.

We estimate the maximum possible bubble displacement D per pulse from the inequality

$$D < V_n T \, \delta_{\text{max}},\tag{7}$$

where T is the pulse width, and where we have assumed $V_p < V_p$. Taking $V_p = 10^3$ cm/s, $\alpha = 0.03$, $R/\nabla = 100$, and $T = 0.5~\mu s$. we find $D < 3~\mu m/p$ ulse consistent with the experimental maximum of about 2 $\mu m/p$ ulse observed.

• Symmetric drive

The foregoing model cannot easily explain those observations of lattice rotation in which sinusoidal ac drive is used. We consider in this case the component of dc lattice rotation arising from the bilinear mixing of radial bubble oscillation and the oscillatory component of the gyrotropic force due to bubble translation.

With this object in mind we incorporate the expression (3) into a dynamical equation

$$-2\pi M_{s}R^{2}\nabla H_{z} = 2\pi M_{s}R(m\dot{\mathbf{V}} + \mu^{-1}\mathbf{V})$$
$$-4\pi SM_{s}\gamma^{-1}\hat{z} \times \mathbf{V}$$
(8)

for translational velocity V. Here ∇H_z is the two-component gradient of the net normal-field component, with respect to displacement in the film plane, $2M_sm$ is the effective mass per unit wall surface, and $\mu = \Delta \gamma / \alpha$ is the conventional mobility. The dynamical equation for R will now be considered.

The equation (8) balances the total magnetostatic force, appearing on the left, with the dynamic reaction appearing on the right. The latter consists of three terms: the reaction due to effective mass, the linear drag, and the gyrotropic deflection force, in the order shown. This equation is considered to apply to any one of the bubbles in an interacting lattice. Thus $H_z(x, y, z, t)$ is considered to include the instantaneous stray field due to the presence of all the other bubbles. In this consideration, coercivity is neglected because it does not play an essential role. However, it is essential to consider oscillations of the radius R because of their nonlinear coupling to the translation V. Thus we write each time dependent variable as a sum of constant and sinusoidal terms

$$\mathbf{F} \equiv \nabla H_z = \mathbf{G}_0 + \operatorname{Re} \mathbf{G}_\omega e^{i\omega t}, \tag{9}$$

$$\mathbf{V} \equiv \dot{\mathbf{X}} = \mathbf{V}_0 + \operatorname{Re} i\omega \mathbf{X}_{\omega} e^{i\omega t}$$
, and (10)

$$R = R_0 + \operatorname{Re} R_{\omega} e^{i\omega t}, \tag{11}$$

where G_{ω} , X_{ω} , and R_{ω} are complex amplitudes of sinusoidal oscillation, and Re means "real part of."

In order to minimize the algebra leading to an expression for V_0 , the constant term in V(t), it is helpful to factor R from Eq. (8). Removing other common factors as well and neglecting H_c , one finds the expression

$$R \nabla H_z = -m\dot{\mathbf{V}} - \mu^{-1}\mathbf{V} + (2S/\gamma R)\hat{z} \times \mathbf{V}. \tag{12}$$

We approximate R^{-1} with R_0^{-1} $(1 - R_0^{-1} \text{Re} R_\omega e^{i\omega t})$ and substitute this and Eqs. (9), (10), and (11) in Eq. (12). Balancing the time-independent terms in the expanded equation, one finds the relation

$$R_{0}G_{0} + \frac{1}{2}(ReR_{\omega}^{*}G_{\omega}) - (S\omega/\gamma R_{0}^{2}) \operatorname{Im} R_{\omega}^{*} \hat{z} \times \mathbf{X}_{\omega}$$
$$= -\mu^{-1}\mathbf{V}_{0} + (2S/\gamma R_{0})\hat{z} \times \mathbf{V}_{0}, \tag{13}$$

where Im means "imaginary part of." We have arranged the terms here in such a way that the total effective zero-frequency drive stands on the left of the equal sign and the steady velocity V_0 on the right.

Now consider the geometry of a rotating lattice. Denote vector components which are radial and aximuthal with respect to the rotating lattice center with the subscripts ρ and ϕ , respectively. Obviously we have

$$V_{0a} = 0$$
, $G_{\omega a} = 0$, and $\pm V_a = V_{\phi} = \rho \Omega$,

where Ω is the circular rotational frequency. Also, by symmetry the contribution to $G_{0\phi}$ from the applied drive field must vanish, so that only a static term $G_{\phi int}$ due to interbubble interactions remains. In component form Eq. (13) reads:

$$RG_0 + \frac{1}{2}(\text{Re}R_{\omega}^*G_{\omega}) + (S\omega/\gamma R_0^2) \text{ Im } R_{\omega}^*X_{\omega\phi}$$

= $-(2S/\gamma R_0)V_{\phi\phi};$ (14)

$$\rho\Omega = (S\omega\mu/\gamma R_0^2) \operatorname{Im} R_\omega^* X_{\omega \alpha} - \mu R_0 G_{\text{dint}}. \tag{15}$$

Equation (14) expresses the fact that, in the steady state, the radial position of a bubble is established by a balance of certain effective radial forces including those caused by mixing of radial and translational oscillations. Equation (15) attributes the rotation to an effective drive force originating from the nonlinear coupling of the assumed bubble-radius oscillation R_{ω} to the lattice-radial component of translational oscillation $X_{\omega\rho}$ through the gyrotropic effect.

The term $G_{\phi \text{int}}$ (ρ) obviously cannot by itself accomplish the rotation, by conservation of energy. To be explicit, consider the domains to be distributed continuously and uniformly. Then the torque on the bubble array, which must vanish, is proportional to $\int_0^{\Re} \rho^2 G_{\phi \text{int}} d\rho$, where \Re is the radius of the lattice. Applying this condition to Eq. (15) we have

$$\mathscr{R}^4 \Omega = (4S\omega\mu/\gamma R_0^2) \int_0^R \rho^2 \operatorname{Im} R_\omega^* X_{\omega\phi} d\rho.$$
 (16)

The mechanism represented by Eq. (16) is explained with the help of Fig. 7(d). Suppose there is a 90° phase lag between X_{ρ} and R so that R is a maximum or minimum whenever X_{ρ} is at a node. Because the drag on the domain is proportional to R, the gyrotropic deflection force is more effective when R is small and \dot{X}_{ρ} is positive

than when R is large and \dot{X}_{ρ} is negative. Thus dX_{ϕ}/dX_{ρ} is a bit greater when \dot{X}_{ρ} is positive and a net increase in X_{ϕ} occurs in every cycle.

The problem remains to calculate R_{ω} and $X_{\omega\rho}$ for substitution into Eq. (16). These quantities may be written as linear combinations,

$$X_{\rho} = \operatorname{Re} \sum_{k} A_{k} u_{k}, \qquad R = R_{0} + \operatorname{Re} \sum_{k} B_{k} u_{k}, \qquad (17)$$

of the normal modes of bubble-lattice vibration u_k . Here A_k and B_k are real constants. The normal modes u_k satisfy equations of motion having the usual form:

$$\ddot{u}_k + \beta_k \dot{u}_k + \omega_k^2 u_k = F_{k\omega} e^{i\omega t}, \tag{18}$$

where β_k is a damping coefficient, ω_k is the circular resonant frequency, and $F_{k\omega}$ the amplitude of the effective driving force. The $F_{k\omega}$ may be assumed to be real because they are in phase with the drive current. The steady state solution is

$$u_k = F_{k\omega} e^{i\omega t} / (\omega_k^2 - \omega^2 + i\omega \beta_k). \tag{19}$$

The effective mean bubble drive, appearing in the integrand of Eq. (16) and which gives rise to the lattice rotation, is proportional to

$$\omega \text{Im } R_{\omega}^* X_{\omega \rho} =$$

$$\omega \sum_{k,\ell} \frac{(A_k B_\ell - B_k A_\ell) F_{k\omega} F_{\ell\omega} \beta_k (\omega_\ell^2 - \omega^2)}{\left[(\omega_k^2 - \omega^2)^2 + \omega^2 \beta_k^2 \right] \left[(\omega_\ell^2 - \omega^2)^2 + \omega^2 \beta_\ell^2 \right]}. \tag{20}$$

From the form of this result we infer that the rotational drive has a biresonant character. Since terms in Eq. (20) with k=l vanish, only pairs of distinct normal modes contribute to the rotation. This circumstance arises from the fact that the in-phase components of R_{ω} and $X_{\omega\rho}$ contribute nothing to the effect. A phase difference other than 0 or 180° occurs only if $k \neq l$, that is, if two distinct modes mix.

The spectrum (20) consists of a series of resonant peaks of either sign which are skewed, but only weakly so if $\beta_k \ll \omega_k$. Thus it is qualitatively consistent with the observations shown in Fig. 4(b). In the case of an ideal lattice consisting of identical bubbles, only modes of small wave vector should be excited because the ac drive field varies slowly over the lattice distance. Thus one expects large rotations at small ω , where the "acoustic" modes lie, and near one large frequency where the "optic" mode of vanishing wave vector lies [34].

The fact that the observed spectrum has more structure than one could interpret in this way suggests that the lattice is effectively disordered by the presence of a mixture of different bubble states having varying positions and numbers of vertical or horizontal Bloch lines, and therefore varying values of S. If this is the case, then even a slow spatial variation of drive field excites modes from

all parts of the spectrum. Our observation of many peaks in rotation and absorption is evidence of considerable disorder in the lattice.

Although we cannot estimate directly the frequency ν of rotation, an upper bound is established by the known experimental fact that wall-velocity is limited to a value of the order of 10^3 cm/sec for $V_{\rm p}$ in uniaxial garnet films [17, 35]. We may therefore substitute $|\omega r_{\omega}| \leq V_p$ and $|\omega X_{\rm orb}| \leq V_p$ into Eq. (16) to find

$$\Re\Omega \le 4S\mu V_n^2 / 3\gamma R_0^2 \omega. \tag{21}$$

We take S=1, $\mu=10^3$ cm sec⁻¹ Oe⁻¹, $\gamma=1.5\times10^7$ sec⁻¹ Oe⁻¹, $R_0=2$ μ m, $\omega=2\times10^7$ radians/s. Thus we find the bubble velocity at the rim limited by $\Omega \leq 100$ cm/s. In our ac experiment, $\mathcal{R}=10^{-2}$ cm so that rotation frequency should be bound by $\Omega/2\pi \leq 2000$ rev/s. We interpret the fact that the observed rotations do not exceed 30 rev/s as indicating that the oscillating radial and translational velocities of bubbles do not generally attain V_n simultaneously.

With respect to our interpretation, one may legitimately doubt whether the ratio six between the inner diameter of the drive coil and the diameter of the confining circle is small enough for the requisite drive gradient $dH_z/d\rho$ to be significant. On the other hand it must be remembered that the breathing oscillations of bubbles in a finite lattice will themselves give rise to inhomogeneous magnetic dipole fields depending on ρ , and effectively providing a gradient drive. Nonetheless, our models of rotation under asymmetric and symmetric excitations are tentative, pending more conclusive study.

Discussion

Most of the bubble motions investigated in the past have required application of a field gradient with a component parallel to the direction of motion. In devices, moreover, this is the main component and has been required to have a wavelength not greater than the bubble diameter or distance between neighboring bubbles. This paper investigates collective bubble motions that occur in low-damping garnet films by excitation involving homogeneous or nearly homogeneous fields, e.g., bias-field modulations. Their gradients, if significant, are in any case orthogonal to the motion studied. These various motions belong to a new phenomenon we call bubble automotion because the self-propulsion results from coupling of the principal translational degree of freedom of the bubble either with the internal degrees or with the orthogonal component of translation.

In this study we have focused attention on the coherent bubble lattice rotation mode, not only because it is coherent and therefore easiest to characterize, but also because it may provide a means of translating the bubble lattice within the store area of bubble lattice devices. Further studies are now in progress on automotion effects in dilute arrays of bubbles and in isolated bubbles.

The mode of coherent lattice translation, rectilinear or rotational, is determined by the geometry of the lattice isolation structure, e.g., a small (ten percent) edge or step in film thickness that does not impose constraints on the resolution of the fabrication process. In applying the effect to the bubble lattice file, the purpose of the isolation structure is to separate the active storage lattice from surrounding domains so as to provide for "frictionless" lattice translation. Lattice rotation by automotion described in the fourth section has also been observed within annular as well as circular confinements. Rectilinear translation has similarly been observed and recorded along parallel confinements. Again, the nature of the response is sensitive to the bias modulation conditions. Nevertheless, it is evident that both speed and directionality of lattice automotion are controllable, e.g., by means similar to those demonstrated in the third and fourth sections of this paper.

What remains to be investigated in the case of lattices in a single layer film and containing bubbles with different wall states is the question of whether the drive modulation conditions necessary for lattice automotion will disturb the wall states. In the case of the (bistable) dual size bubble states as in the composite layer structure of Lin, et al., we have demonstrated that the storage bubble is not thereby collapsed or modulated. However, we have thus far obtained only preliminary information about the characteristics of lattice rotation in this layered film, e.g., Fig. 6(c), and have not yet demonstrated the high speed rotation that was produced in a single layer film, i.e., Fig. 4(a), using a suitable confinement structure.

Acknowledgments

We gratefully acknowledge P. Gazis for valuable technical assistance, R. L. Anderson for fabricating confinement grooves in garnet films supplied by E. A. Giess, and Y. Lin and E. A. Giess for lending us the composite, trilayer garnet film.

References

- A. H. Bobeck, "Properties and Device Applications of Magnetic Domains in Orthoferrites," *Bell System Tech. J.* 46, 1901 (1967).
- A. H. Bobeck and E. Della Torre, Magnetic Bubbles, North Holland Publishing Co., Amsterdam, 1975. Also, Hsu Chang, Magnetic Bubble Technology: Integrated Circuit Magnetics for Digital Storage and Processing, IEEE Press, New York, 1975.
- O. Voegeli, B. A. Calhoun, L. I. Rosier, and J. C. Slonczewski, "The Use of Bubble Lattices for Information Storage," 20th Annual Conference on Magnetism and Magnetic Materials, San Francisco, AIP Conf. Proc., No. 24, 617 (1975).
- L. I. Rosier, D. M. Hannon, H. L. Hu, L. F. Shew, and O. Voegeli, "Bubble Lattice Translation-Experimental Re-

- sults," 20th Annual Conference on Magnetism and Magnetic Materials, San Francisco, AIP Conf. Proc. No. 24, p. 620 (1975).
- J. C. Slonczewski, A. P. Malozemoff, and O. Voegeli, "Statics and Dynamics of Bubbles Containing Bloch Lines,"
 18th Annual Conference on Magnetism and Magnetic Materials, Denver, AIP Conf. Proc., No. 10, 458 (1972).
- Y. S. Lin, P. J. Grundy, and E. A. Giess, "Bubble Domains in Magnetostatically Coupled Films," Appl. Phys. Lett. 23, 485 (1973); also, Y. S. Lin and P. J. Grundy, "Bubble Domains in Coupled Garnet Films," J. Appl. Phys. 45, 4084 (1974).
- B. E. Argyle and P. Chaudhari, "Dynamic Bubble Array Technique to Detect Defects," 18th Annual Conference on Magnetism and Magnetic Materials, Denver, AIP Conf. Proc., No. 10, 403 (1973).
- 8. B. E. Argyle and P. Chaudhari, "Diffraction of Light Using Magnetic Bubbles," *IBM Tech. Disclosure Bulletin* 18, 603 (1975).
- H. Dötsch and H. J. Schmitt, "Interaction of Microwaves with Ring Domains in Magnetic Garnet Films," Appl. Phys. Lett. 24, 422 (1974); H. Dötsch, "Dynamics of Magnetic Domains in Microwave Fields," Proceedings of the Winter School on New Magnetic Materials. Poland, 1975.
- B. A. Boxall, "Orthogonal Motion of Bubble Domains in Pulsed Field Gradients," *IEEE Trans. Magn.* MAG-10, (1974).
- W. C. Hubbell, "Magnetic Bubble Propagation by Pulsed rf Currents," 20th Annual Conference on Magnetism and Magnetic Materials, San Franciso, AIP Conf. Proc., No. 24, 552 (1974).
- F. G. West and D. C. Bullock, "Further Properties of Hard Bubbles," 18th Annual Conference on Magnetism and Magnetic Materials, Denver, AIP Conf. Proc., No. 10, 483 (1973).
- 13. W. Doyle, private communication, 1972.
- W. J. Tabor, A. H. Bobeck, G. P. Vella-Coleiro, and A. Rosencwaig, "A New Type of Cylindrical Magnetic Domain (Hard Bubble)," 18th Annual Conference on Magnetism and Magnetic Materials, Denver, AIP Conf. Proc., No. 10, 442 (1973).
- A. P. Malozemoff and J. C. Slonczewski, "Wall Motion by In-Plane Field Pulses in Bubble Materials." 20th Annual Conference on Magnetism and Magnetic Materials. San Francisco, AIP Conf. Proc., No. 24, 603 (1975).
- J. C. Slonczewski, "Theory of Bloch-line and Bloch-wall Motion," J. Appl. Phys. 45, 2705 (1974).
- B. E. Argyle and A. Halperin, "A Measuring System for Analysis of AC Domain Wall Motions in Bubble Materials," IEEE Trans. Magn. MAG-9, 238 (1973).
- T. W. Collins and W. Cole, "Simulation of Translation Forces in Cylindrical Magnetic Domains," *IBM J. Res. Develop*, 20, 132 (1976, this issue).
- F. A. De Jonge and W. F. Druyvesteyn, "Calculations and Experiments Related to the Magnetostatics of Bubble Domains," Festkörprobleme XII, 53 (1972).
- R. M. Josephs and B. F. Stein, "The Influence of an In-Plane Field on Bubble Dynamics," 19th Annual Conference on Magnetism and Magnetic Materials, Boston, AIP Conf. Proc., No. 18, 227 (1973).
- R. W. Shaw, J. W. Moody, and R. M. Sandfort, "Dynamic Properties of High Mobility Garnet Films in the Presence of In-Plane Magnetic Fields," J. Appl. Phys. 45, 2672 (1974).
- F. H. de Leeuw and J. M. Robertson, "Observation and Analysis of Magnetic Domain Wall Oscillations in Ga: YIG Film," to be published.
- 23. M. H. H. Höfelt, "Elastic Constants and Wave Phenomena in Bubble Lattices," J. Appl. Phys. 44, 414 (1973).
- 24. M. H. H. Höfelt, "On the Radial Mode in Bubble Lattices," *IEEE Trans. Magn.* 9, 621 (1973).

- 25. A. P. Malozemoff, "Interacting Bloch Lines; a New Mechanism for Wall Energy in Bubble Domain Materials," Appl. Phys. Lett. 21, 149 (1972).
- 26. O. Voegeli and B. A. Calhoun, "Domain Formation and Associated Wall States," IEEE Trans. Magn. MAG-9, 617 (1973).
- 27. B. E. Argyle and J. C. DeLuca, "Magnetic Domain Systems Using Different Types of Domains," U.S. Patent No. 3,911,411, Oct. 7, 1975; B. E. Argyle, "Dual-Bubble Lattice File," IBM Tech. Disclosure Bulletin 17, 3767 (1975).
- 28. W. J. DeBonte, "Static Stability of Half Bubbles," Bell System Tech. J. 51, 1933 (1972).
- 29. T. R. Oeffinger, G. W. Roland, A. I. Braginski, and R. W. Patterson, "Bistable Magnetic Bubbles: Conditions Leading to Stability in LPE Garnet Films," Appl. Phys. Lett. 24, 32 (1974).
- 30. J. Heisma, G. Bartels, W. F. Druyvesteyn, V. Enz J.-P.-Krumme, and A. G. H. Verhulst, "Observation of Various Types of Bubbles Bounded by a Compensation Wall," IEEE Trans. Magn. MAG-10, 630 (1974).
- 31. A. A. Thiele, "Steady-State Motion of Magnetic Domains," Phys. Rev. Lett. 30, 230 (1973).

- 32. A. P. Malozemoff, "Mobility of Bubbles with Small Numbers of Bloch Lines," J. Appl. Phys. 44, 5080 (1973).
- R. W. Patterson, J. Appl. Phys. 45, 5018 (1974).
 M. M. Sokoloski and T. Tanaka, "Excitation Spectra of Magnetic Bubble Lattices," J. Appl. Phys. 45, 3091 (1974).
- 35. B. E. Argyle, J. C. Slonczewski, and A. F. Mayadas, "Domain Wall Motion in Rare-Earth Substituted Ga: YIG Epitaxial Films," 17th Annual Conference on Magnetism and Magnetic Materials, Chicago, AIP Conf. Proc., No. 5, 175 (1971).

Received June 27, 1975

B. E. Argyle and J. C. Slonczewski are located at the IBM Thomas J. Watson Research Center, Yorktown Heights, New York 10598. O. Voegeli is at the General Products Division Laboratory, Monterey and Cottle Roads, San Jose, California 95193.